International Journal for Housing Science and Its Applications
Publish August 6, 2025. Volume 46, Issue 3 Pages 4885-4894

https://doi.org/10.70517/ijhsa463418

Combining physical simulation and statistical modeling methods to study the spatial distribution of immune cells in lung cancer microenvironment

Jianming Peng[1], Youai Dai[2], Huishen Yan[1] and Rui Liang[3,*]
[1] Shool of Medicine, Yangzhou Polytechnic College, Yangzhou, Jiangsu, 225009, China
[2] Laboratory of Organ Transplantation Research Institute, Wuxi People's Hospital Affiliated to Nanjing Medical University, Wuxi, Jiangsu, 214023, China
[3] Shool of Basic Medical Science, Suzhou Vocational Health College, Suzhou, Jiangsu, 215009, China
Corresponding authors: (e-mail: pengjianming2025@163.com).

Abstract The spatial distribution characteristics of immune cells in the lung cancer microenvironment profoundly affect tumor progression and immunotherapy efficacy. In this paper, we integrate physical simulation and statistical modeling to systematically investigate the dynamic interactions and spatial distribution of immune cells in the tumor microenvironment of non-small cell lung cancer (NSCLC). A system of partial differential equations (PDEs) was constructed based on statistical methods to simulate the formation mechanism of the immunosuppressive microenvironment during tumor growth. The cell kinetic behavior in non-equilibrium state was portrayed by ODE kinetic model to reveal the characteristics of spatial distribution of immune cells. Flow cytometry and spatial parameter analysis of clinical samples were combined to quantify the spatial distribution pattern of M2 macrophages and IL-10$^+$NK cells. It was found that the mean density, mean minimum proximity distance, and effective percentage of CD68$^+$ TAMS were significantly higher than those of CD163$^+$ TAMS and IRF8$^+$ TAMs in the subpopulations of patient TAMs (CD68$^+$, CD163$^+$, and IRF8$^+$), and that M2 macrophages and IL-10$^+$NK cells differed in their proportions and functional inhibitory status in different tissues.

Index Terms non-small cell lung cancer, lung cancer microenvironment, partial differential equations, ODE kinetic model, spatial distribution of immune cells

I. Introduction

Lung cancer is one of the most common malignant lung cancers and one of the leading causes of cancer death worldwide [1], [2]. When the body encounters lung cancer, the body's immune system works to enhance its defense mechanisms [3]. Immune cells play an indispensable role in this regard, providing support and guidance to the body in fighting cancer cells [4], [5]. However, modern medicine has discovered that lung cancer is not only a problem posed by cancer cells, but that immune cells and their spatial distribution in the lung cancer microenvironment also play a critical role [6], [7].

The lung cancer microenvironment is composed of cancer cells, immune cells, vascular endothelial cells, fibroblasts and stromal cells, etc. The formation of the microenvironment can be realized by the infiltration of immune cells induced by cancer cells [8]-[10]. Several types of immune cells, including T cells, B cells, macrophages, and dendritic cells, are present in the lung cancer microenvironment [11], [12]. These immune cells, play an important role in immune surveillance and anti-lung cancer immune response in lung cancer [13]. Immune cell infiltration is the key to anti-lung cancer immunotherapy, and immune cell infiltration in the microenvironment of lung cancer is closely related to the prognosis of lung cancer, with a relatively high number of immune cell infiltration in patients with benign lung cancer, and a significant decrease in the number of immune cell infiltration in patients with malignant lung cancer [14]-[17]. As a result, immune cells in the microenvironment of lung cancer became a hot area of cancer research [18]. Researchers have begun to study these immune cells to explore their role in the lung cancer microenvironment and to hypothesize about their interactions with the human immune system in order to seek a new approach to cancer therapy [19]-[21].

In this paper, we first construct a partial differential equation model to simulate the dynamic process of cells in TME based on the law of mass action and the assumption of spherical symmetry. The formation of tumor necrotic core is characterized by boundary conditions and initial parameter settings. Separate the deterministic dynamics from stochasticity to resolve the potential function characteristics of the spatial distribution of immune cells and the mechanism of steady state transition. Taking 50 NSCLC patients from a hospital as study samples, double-ended PE100 sequencing was used to detect the quality of the samples. The cells were labeled into different subjects by

cell markers to realize the cell grouping of clinical samples. The distribution patterns of the three subpopulations were analyzed by combining the clinicopathological characteristics of the patients and the density and spatial distribution parameters of the TAMs of the three subpopulations. Flow cytometry was used to analyze single-cell suspensions from each tissue to explore the spatial distribution heterogeneity of M2 macrophages and IL-10^{+}NK cells.

II. Non-small cell kinetic simulation of lung cancer microenvironment based on statistical modeling

Non-small cell lung cancer (NSCLC) is one of the leading causes of cancer-related deaths worldwide. Despite significant advances in diagnosis and treatment, the overall prognosis of NSCLC patients remains poor. The immunosuppressive environment in the tumor microenvironment is an important reason for the failure of immunotherapy, and an in-depth study of the distribution mechanism of immune cells in the NSCLC tumor microenvironment can provide a theoretical basis for the development of new immunotherapy strategies.

In this paper, we combine physical simulation and statistical modeling to establish a multi-scale model to explore the law of immune cell spatial distribution.

II. A.Mathematical modeling of the tumor microenvironment

II. A. 1) Assumptions for model application

During tumor growth, biological processes between different classes of cells ensure continuous changes in the tumor microenvironment, which subsequently lead to different processes such as tumor growth, metastasis, adhesion, invasion and angiogenesis. The model in this paper focuses on simulating the interactions of four types of cells in the microenvironment, namely tumor cells, immune cells, cancer-associated fibroblasts (CAFs), and angiogenic cells. Experiments have confirmed that these four types of cells are the main components of the TME and are direct participants in the functions of immune function, tumor promotion, and material transport, respectively, during tumor development.

Generally, the proliferation of tumor cells causes the inner cells of the tumor to exert an outward force on the outer cells, at which time the outer layer of cells will move relatively outward with the expansion of their size, and this is the reason why the tumor volume keeps getting larger. In other works, the shape of the tumor growth is usually approximated as a sphere, which is to facilitate the calculation and analysis, so this is also set in this paper. The modeling in this paper follows the following assumptions:

(1) The shape of a solid tumor is a radially symmetric sphere containing free boundaries and has a uniform density.

(2) During tumor growth, the number of angiogenic cells and cancer-associated fibroblasts varies with the number of tumor cells.

(3) The spreading effect of cancer-associated fibroblasts and angiogenic cells is ignored in the model.

(4) Immune cells can be recruited by tumor cells and spread from the outside to the inside of solid tumors.

II. A. 2) Mathematical form of the model

In this paper, we mainly consider the biological interactions processes in the tumor microenvironment to establish a mathematical model. Based on the Mass action theorem in biochemical reactions, this paper uses a system of partial differential equations to portray the dynamics of four types of cells in the tumor microenvironment, where the four cellular variables are: tumor cells $([C])$, immune cells $([E])$, cancer-associated fibroblasts $([F])$ and angiogenic cells $([A])$. The change in the number of tumor cells over time is the change in the number of tumor cells by free diffusion minus the change in the number of tumor cells by convection, the killing of tumor cells by immune cells, and the necrotic nuclear portion of tumor cells, plus the proliferation of tumor cells. The amount of change in the number of immune cells over time was the amount of change in the number of immune cells with free diffusion plus the activation of immune cells and the recruitment of immune cells by tumor cells, minus the amount of change in the number of immune cells with convection. The amount of change in the number of cancer-associated fibroblasts over time is the amount of change in the generation of CAFs by tumor cells encroaching on tissue plus the generation of CAFs by tumor cells encroaching on tissue, minus the amount of change in CAFs with convection. The amount of change in the number of angiogenic cells over time is equal to the proliferation of angiogenic cells minus the amount of change in angiogenic cells with convection.

After clarifying the various components in the model, it was further translated into the mathematical language of formulas as follows:

$$\frac{\partial[C]}{\partial t}+\underbrace{\nabla\cdot([C]\cdot u)}_{convection}=\underbrace{D_C\Delta[C]}_{diffusion}+\underbrace{\sigma_1\left(1+\frac{[F]}{[C]+p}\right)\left(1-\frac{[C]}{k}\right)[C]}_{logistic}-\underbrace{\lambda\left(1-\frac{[F]}{[C]+p}\right)[C][E]}_{immune}-\underbrace{\tau\beta\left(1-\frac{[A]}{\theta_2[C]+p}\right)[C]}_{necrotic\ nucleus} \tag{1}$$

$$\frac{\partial[E]}{\partial t}+\underbrace{\nabla\cdot([E]\cdot u)}_{convection}=\underbrace{D_E\Delta[E]}_{diffusion}+\underbrace{\gamma(E^*-[E])}_{activation}+\underbrace{\delta_1\frac{[C]}{g+[C]}[E]}_{tumor\ attraction} \tag{2}$$

$$\frac{\partial[F]}{\partial t}+\underbrace{\nabla\cdot([F]\cdot u)}_{convection}=\underbrace{\alpha f([C])}_{tumor\ erosion}+\underbrace{\delta_2\frac{[C]}{g+[C]}(\theta_1[C]-[F])}_{BMC\ differentiation} \tag{3}$$

$$\frac{\partial[A]}{\partial t}+\underbrace{\nabla\cdot([A]\cdot u)}_{convection}=\underbrace{\sigma_2(\theta_2[C]-[A])}_{dynamic\ growth} \tag{4}$$

Based on the assumption that tumor growth is approximated as a sphere, the PDEs model described above can be further transformed into a form in spherical coordinates:

$$\frac{\partial[C]}{\partial t}+\underbrace{\frac{1}{r^2}\frac{\partial}{\partial r}(r^2[C]u)}_{convection}=\underbrace{D_C\frac{1}{r^2}\frac{\partial}{\partial r}\left(r^2\frac{\partial[C]}{\partial r}\right)}_{diffusion}+\underbrace{\sigma_1\left(1+\frac{[F]}{[C]+p}\right)\left(1-\frac{[C]}{k}\right)[C]}_{logistic}-\underbrace{\lambda\left(1-\frac{[F]}{[C]+p}\right)[C][E]}_{immune}-\underbrace{\tau\beta\left(1-\frac{[A]}{\theta_2[C]+p}\right)[C]}_{necrotic\ nucleus} \tag{5}$$

$$\frac{\partial[E]}{\partial t}+\underbrace{\frac{1}{r^2}\frac{\partial}{\partial r}(r^2[E]u)}_{convection}=\underbrace{D_E\frac{1}{r^2}\frac{\partial}{\partial r}\left(r^2\frac{\partial[E]}{\partial r}\right)}_{diffusion}+\underbrace{\gamma(E^*-[E])}_{activation}+\underbrace{\delta_1\frac{[C]}{g+[C]}[E]}_{tumor\ attraction} \tag{6}$$

$$\frac{\partial[F]}{\partial t}+\underbrace{\frac{1}{r^2}\frac{\partial}{\partial r}(r^2[F]u)}_{convection}=\underbrace{\alpha f([C])}_{tumor\ erosion}+\underbrace{\delta_2\frac{[C]}{g+[C]}(\theta_1[C]-[F])}_{BMC\ differentiation} \tag{7}$$

$$\frac{\partial[A]}{\partial t}+\underbrace{\frac{1}{r^2}\frac{\partial}{\partial r}(r^2[A]u)}_{convection}=\underbrace{\sigma_2(\theta_2[C]-[A])}_{dynamic\ growth} \tag{8}$$

Among them:

$$\beta=\begin{cases}0, & when\ ([C]\cdot10^{-6})^{1/3}\le0.26\\ \left(\dfrac{([C]\cdot10^{-6})^{1/3}-0.26}{([C]\cdot10^{-6})^{1/3}}\right)^3, & when\ ([C]\cdot10^{-6})^{1/3}\ge0.26\end{cases} \tag{9}$$

$$f([C]) = \underbrace{\sigma_1\left(1+\frac{[F]}{[C]+p}\right)\left(1-\frac{[C]}{k}\right)[C]}_{logistic} \\ \underbrace{-\lambda\left(1-\frac{[F]}{[C]+p}\right)[C][E]}_{immune} \underbrace{-\tau\beta\left(1-\frac{[A]}{\theta_2[C]+p}\right)[C]}_{necrotic\ nucleus} \tag{10}$$

The convective velocity $u = u(r,t)$ in the model represents the cell movement velocity at t and position r, which is generated mainly because of cell proliferation and apoptosis; cell proliferation velocity greater than the death velocity indicates the expansion of the tumor volume, which corresponds to a cell movement velocity greater than 0, and cell death velocity greater than the proliferation velocity corresponds to a cell movement velocity less than 0.

According to the model assumption, the cell density inside the solid tumor is fixed, so the sum of the number of the four types of cells per unit volume is a constant value, i.e.:

$$[C]+[E]+[F]+[A] = \theta \tag{11}$$

In the numerical solution process of this paper the model is calculated in spherical coordinates, however, the unit of the four variables is the number of cells, so in order to satisfy the assumption of density invariance, this paper sets the cell density constant in Equation (11) to be $\theta = \theta(h,R)$, in which h and R denote the spatial intervals of numerical calculations as well as the radius of the tumor, respectively.

Early tumor growth is in the stage of avascular growth, when the growth of tumor cells mainly relies on the nutrients in the surrounding environment, and the tumor grows more slowly. When the solid tumor grows to a certain size, because there is no other source to provide nutrients to the tumor cells, the cells inside the tumor body will stop growing or even die, forming a necrotic core, so that the tumor at this stage usually has a diameter of no more than 2mm.

The model in this paper portrays the tumor growth of a sphere containing a free boundary, whose internal boundary $\Gamma_{inner}\left(r = R_{inner}(t)\right)$ is the boundary of the necrotic core and the proliferating cell layer, and the external boundary $\Gamma_{outer}\left(r = R(t)\right)$ is the outer surface of the tumor volume, and the structure of the sphere tumor is shown in Figure 1. The variation of the external boundary, in turn, can be represented by the convection velocity:

$$\frac{dR}{dt} = u(R(t),t) \tag{12}$$

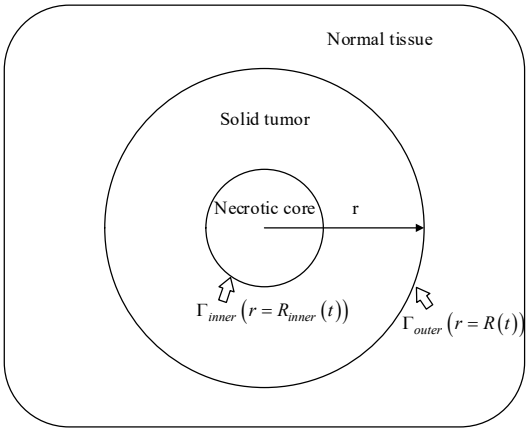

Figure 1: Structure of the spheroid tumor

Combining the exchange and movement of the four types of cells in the microenvironment, the boundary conditions of the model in this paper have the following settings:

$$[C] = 0 \ on\ \Gamma_{inner} \ and \ \frac{\partial[C]}{\partial r} = 0 \ on\ \Gamma_{outer} \tag{13}$$

$$[E]=0 \ on \ \Gamma_{inner} \ and \ [E]=E_s \ on \ \Gamma_{outer} \tag{14}$$

$$[F]=0 \ on \ \Gamma_{inner} \ and \ \frac{\partial[F]}{\partial r}=0 \ on \ \Gamma_{outer} \tag{15}$$

$$[A]=0 \ on \ \Gamma_{inner} \ and \ \frac{\partial[A]}{\partial r}=0 \ on \ \Gamma_{outer} \tag{16}$$

where E_s denotes the number of immune cells recruited or activated at the outer boundary of the tumor. In addition, the initial value of the model is set to:

$$\begin{aligned}[C](r,0)=C_0,[E](r,0)=E_0,[F](r,0)=F_0,[A](r,0)\\ =A_0,R_{inner}(0)<r<R(0)\end{aligned} \tag{17}$$

II. B.ODE kinetic modeling of non-small cell lung cancer

ODE kinetic modeling, a set of coupled nonlinear ordinary differential equations describes the regulatory relationships between endogenous factors in a network. From a physical point of view, the onset and progression of complex diseases such as cancer are typically non-equilibrium processes. In this paper, we develop a general framework for the study of non-equilibrium processes in non-equilibrium processes using nonlinear stochastic differential equations (Lang's van equations in their generalized form in physics). By combining the original stochastic dynamical equations:

$$\frac{dx_i}{dt}=f_i(X,\alpha)+\zeta_i(X,t)\left(Which \ X=\left(x_1,x_2,\cdots,x_n\right)^T\right) \tag{18}$$

The decomposition into three components - the friction matrix $S(x)$, the antisymmetric transverse matrix $A(x)$, and the potential function $\phi(x,\alpha)$ - is obtained:

$$\sum_j\left[s_{ij}(X)+A_{ij}(X)\right]\frac{dx_j}{dt}=-\frac{\partial\phi(X,\alpha)}{\partial x_i}+\xi_i(X,t) \tag{19}$$

where ξ is 0 indicating that the white noise satisfies the approximate relation $\langle\xi_i(X,t)\xi_j(X,t')\rangle=2\in S_{ij}(X)\delta(t-t')$.

Morphing from Eq. (18) to Eq. (19), the deterministic and stochastic parts correspond individually to produce two relations, with the stochastic part leading to the generalized Einstein relation:

$$\sum_{s,t}\left[S_{is}(X)+A_{is}(X)\right]D_{st}(X)\left[S_{tj}(X)+A_{tj}(X)\right]=S_{ij}(X) \tag{20}$$

Provides $n(n+1)$ equations when $i\geq j$; deterministic partially induced:

$$\sum_j\left[S_{ij}(X)+A_{ij}(X)\right]D_{st}(X)\left[S_{tj}(X)+A_{tj}(X)\right]=-\partial_i\phi(X,\alpha) \tag{21}$$

A potential function with zero spin can be obtained:

$$\begin{aligned}&\partial_i\sum_s\left\{\left[S_{js}(X)+A_{js}(X)\right]f_s(X,\alpha)\right\}\\&-\partial_j\sum_t\left\{\left[S_{it}(X)+A_{it}(X)\right]f_s(X,\alpha)\right\}=0\end{aligned} \tag{22}$$

When $i>j$ gives $n(n-1)/2$ equations. These n^2 equations determine the n^2 unknowns in $S(X)+A(X)$ under appropriate boundary conditions, and then the potential function $S(X)+A(X)f(X,\alpha)$.

The corresponding Fokker-Planck equation of Eq. (19) is:

$$\partial_t\rho(X,t)=\sum\partial_i\left[D_{ij}(X)+Q_{ij}(X)\right]\left[\partial_j\phi(X,\alpha)+\varepsilon\partial_j\right]\rho(X,t) \tag{23}$$

where $Q(X)$ is the antisymmetric matrix determined by $[D(X)+Q(X)]=[S(X)+A(X)]^{-1}$. Thus, relating the smooth probability density function $\rho(X)$ in phase space to the potential function $\phi(x,\alpha)$, $\rho(X)\propto\exp\left[-\frac{\phi(x,\alpha)}{\varepsilon}\right]$. The matrices S, A, D and Q may also depend on α. When $\varepsilon\to 0$, $dx_i/dt=f_i$, and thus the potential function ϕ is also deterministically corresponding to the Lyapunov function of the dynamics.

$$\begin{aligned}\frac{d\varnothing(x,\alpha)}{dt}&=-\sum_i\partial_i\varnothing(x,\alpha)\frac{dx_i}{dt}\\&=-\sum_{ij}\left[S_{ij}(X)+A_{ij}(X)\right]f_i(X,\alpha)f_j(X,\alpha)\\&=-\sum_{ij}S_{ij}(X)f_i(X,\alpha)f_j(X,\alpha)\le 0\end{aligned}\tag{24}$$

The kinetic equivalence of the potential function to the Lyapunov function is further demonstrated, and the correspondence between the deterministic steady state and the stochastic localized most probable state is obtained.The decomposition has its applications in engineering and physics.Mathematically, our method can be thought of as a stochastic integral of the A type using stochastic differential equations. The A-type integral solution can be derived physically by taking the zero-mass limit of the noise-containing 2n-dimensional Newtonian equation and the corresponding Klein-Kramers equation. On the other hand, applying the traditional Ito or Stratonovich interpretation, we observe that even for additive noise (constant diffusion matrix D) there may be an inconsistency between stochastic and deterministic dynamics. The bridge between stochastic and deterministic dynamics is built within our framework: stable states obtained from deterministic partial differential equations can be directly interpreted as local maxima of the distribution of stable states, and stochastic transfers between locally most probable states can be viewed as transfers between corresponding stable states. Thus, the potential landscape under A-type integral solutions is robust with respect to noise. Note that in many previous studies using conventional Ito or Stratonovich integrals, the existence of such robustness is also assumed, e.g., the computation of the potential difference between a given steady state and a transition state by path integrals obtained from deterministic equations without taking into account the positional bias can give rise to complications and erroneous results when the noise intensity is not sufficiently small.

In the following exposition, we omit the explicit dependence of the noise and perform a A-type stochastic integration of f_i in Eq. (18) to obtain Eq. (25):

$$\frac{dx_i}{dt}=\frac{\sum_u a_{iu}\cdot x_u^{n_{iu}}}{1+\sum_u a_{iu}\cdot x_u^{n_{iu}}}\times\frac{1}{1+\sum_v a_{iv}\cdot x_v^{n_{iv}}}-x_i\tag{25}$$

At this point, we obtain a set of ordinary differential equations (ODEs) with the above form to approximate the activation-inhibition-regulation relationship of the factors in the network. On the right-hand side of the equations, the first term describes the generation rate of the factor in the form of the product of Hill functions; the second term represents the degradation rate of the factor, and the last term is the original content of the factor at the moment t, with the coefficients n and a in the equations representing the Hill coefficients and dissociation constants, respectively.

III. Spatial distribution of immune cells in the microenvironment of lung cancer in clinical samples

NSCLC is one of the leading causes of cancer-related deaths worldwide, accounting for approximately 85% of all lung cancer cases. Although targeted therapies and immunotherapies have shown good efficacy in some NSCLC patients, the overall prognosis of NSCLC patients remains poor. The immunosuppressive environment in the tumor microenvironment is one of the major reasons for the failure of immunotherapy. Tumor cells evade the surveillance of the immune system by expressing immune checkpoint molecules and inducing immunosuppressive cell aggregation, etc. The complexity of these immune escape mechanisms increases the difficulty of immunotherapy and is a therapeutic dilemma that needs to be overcome at present. Therefore, an in-depth study of immune cell functions in the NSCLC tumor microenvironment is important for improving therapeutic strategies.

M2 macrophages and IL-10$^+$NK cells, as key immune components in the tumor microenvironment, play a role in promoting tumorigenesis and progression.M2 macrophages have immunosuppressive functions and can promote

tumor growth, angiogenesis, and tumor metastasis.TAMs usually exhibit M2 macrophage phenotypic and functional characteristics.

NK cells are an important component of the innate immune system and have the ability to directly kill tumor cells. Tumor cells can limit the function of NK cells in the tumor microenvironment by upregulating inhibitory ligands or secreting immunosuppressive factors.

Both $CD206^{+}IL\text{-}10^{+}$M2 macrophages and $IL\text{-}10^{+}$NK cells in the tumor microenvironment secrete IL-10 and inhibit the function of antigen-presenting cells.IL-10 not only promotes the polarization of TAMs toward the M2-type and inhibits their antitumor response, but also inhibits NK cell activation, weakening their anti-tumor activity. However, the interrelationship between M2 macrophages and $IL\text{-}10^{+}$NK cells in the NSCLC tumor microenvironment is unclear.

III. A. Selection and processing of sample data

III. A. 1) Sample Sources

In this study, 50 patients with NSCLC, including 28 cases of squamous cell carcinoma and 22 cases of adenocarcinoma of the lung, who were first diagnosed with lung cancer, did not receive any other therapeutic interventions, and excluded from other diseases in a hospital, were recruited. All patients were staged by TNM staging system based on pathological diagnosis and clinical characterization. Flow-through specimens were rapidly transferred to 50 ml sterile centrifuge tubes containing F12 medium in an isolated sterile environment to make single-cell suspensions, stained, and mounted. Each specimen was uniquely coded and the coding did not divulge any donor information to ensure privacy, and this study was approved by the hospital ethical review board.

III. A. 2) Quality testing

Quality testing of the samples is required before formal sequencing on the machine, and this sequencing was performed by double-ended PE100 sequencing, and the standard size of WTA-Index should be around 450 bp, and the standard size of ST-Index should be around 290 bp. The test results showed that the WTA-Index and ST-Index of all samples met the quality testing requirements. The detection results of three of the samples are shown in Figure 2(a~b), and the sequencing peaks of each WTA-Index sample are around 450bp, and the sequencing peaks of ST-Index samples are around 290bp.

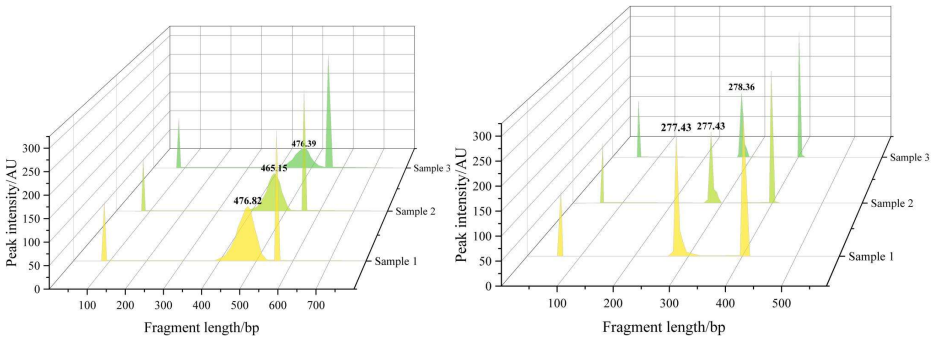

(a)WTA-Index (b)ST-Index

Figure 2: Test results of WTA-Index and ST-Index (Part)

III. A. 3) Cellular compartmentalization

Cells were labeled into different subjects by cell markers, and oligodendrocytes were obtained according to the marker genes OLIG2, PLP1, MBP, TUBB4A, TF, APLP1, CNPMAG, CRYAB, PTGDS, and CNDP1. Glioblastoma cells were obtained according to marker genes PTPRZ1, GFAP, FABP7. Endothelial cells were obtained according to marker genes CD34, CD31, CDH5, CLDN5, FLT1. Immune cells were obtained according to the marker genes PTPRC, CD3, CD74, HLA-DRA, CCL3, IL1B. Pericytes were obtained according to marker genes RGS5, MCAM, CSPG4. The results of cell fractionation were shown in Figure 3, the tumor microenvironment contained cells divided into five categories of subject cells, as normal nervous system cells, tumor cells, endothelial cells, immune cells, and peripheral skin cells, with a total of 127,450 cells.

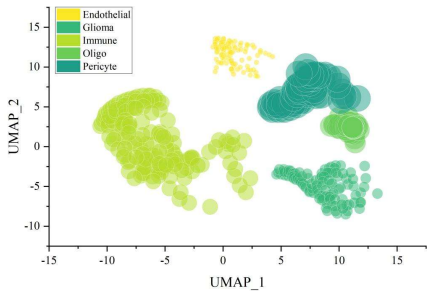

Figure 3: Cell clustering results

The 5 classes of subject cell markers are shown in Figure 4 and correspond to the actual marker genes, further confirming the accuracy of the subject cell compartmentalization.

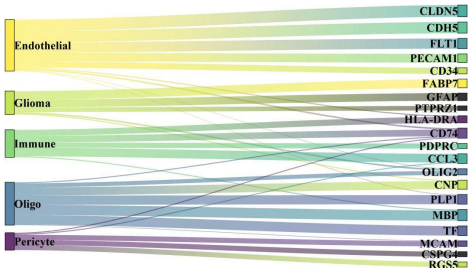

Figure 4: Cell markers of the five classes of subjects

Table 1: Clinicopathological characteristics

Characteristic		Number of patients(%)
Gender	Male	48
	Female	52
Preoperative neurological dysfunction	No	32
	Yes	68
Tumor location	Axial	36
	Extra-axial	64
Recurrence during follow-up	No	32
	Yes	68
Campanacci stage	Ⅰ	12
	Ⅱ	36
	Ⅲ	52
Characteristic		Density(cells/mm²)
$CD68^+$		362.5±288.1
$CD163^+$		97.8±118.9
$IRF8^+$		109.5±126.4
Characteristic		Average minimum proximity distance(μm)
$CD68^+$		197.9±144.7
$CD163^+$		38.2±24.5
$IRF8^+$		50.9±23.7
Characteristic		Effective percentage(%)
$CD68^+$		28.66±20.1
$CD163^+$		17.2±9.4%
$IRF8^+$		8.1±6.5

III. B. TAMs density and spatial distribution parameters

In this paper, the demographic information, clinicopathological characteristics, and density and spatial distribution parameters of TAMs in three subgroups of 50 patients were counted, and the statistical results are shown in Table 1. The results of the visualization of the density and spatial distribution parameters of TAMs of the three subgroups

are shown in Figure 5. The average densities of CD68⁺ TAMS, CD163⁺ TAMS, and IRF8⁺ TAMs in patients were 362.5±288.1/mm², 97.8±118.9/mm², and 109.5±126.4/mm², respectively. The average minimum proximity distances were 197.9±144.7 μm, 38.2±24.5 μm, and 50.9± 23.7 μm. The effective percentages were 28.66±20.1%, 17.2±9.4%, and 8.1±6.5%, respectively. It can be seen that the mean density, mean minimum neighbor distance, and effective percentage of CD68⁺ TAMS were significantly higher than those of CD163⁺ TAMS and IRF8⁺ TAMs in patients.

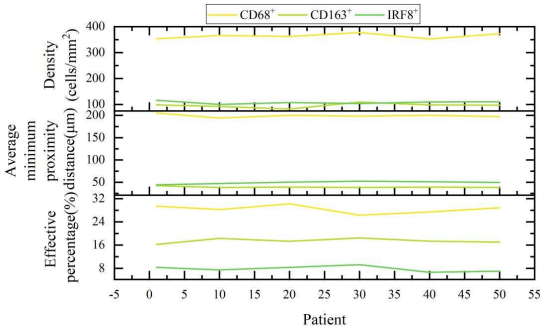

Figure 5: Density and spatial distribution parameters of TAMs in the three subgroups

III. C. Spatial distribution patterns of M2 macrophages and IL-10NK+ cells

To further investigate whether there were differences in the spatial distribution characteristics between M2 macrophages and IL-10NK+ cells, the analysis was carried out using flow cytometry. The proportions and numbers of M2 macrophages and IL-10NK+ cells in each tissue are shown in Figure 6 (a~b), respectively. The analysis of flow cytometry results showed that the proportions of M2 macrophages and IL-10NK+ cells were significantly different in each tissue. The epithelial and lamina propria of duodenum, jejunum, and ileum had more than 60% of M2 macrophages, while the proportions of M2 macrophages, IL-10NK+ cells were similar in blood-related tissues and lymph node tissues. In addition, there were some differences in the number of M2 macrophages and IL-10NK+ cells isolated and purified from different tissues by flow cytometry counting, and the highest numbers of M2 macrophages and IL-10NK+ cells were found in spleen tissues.

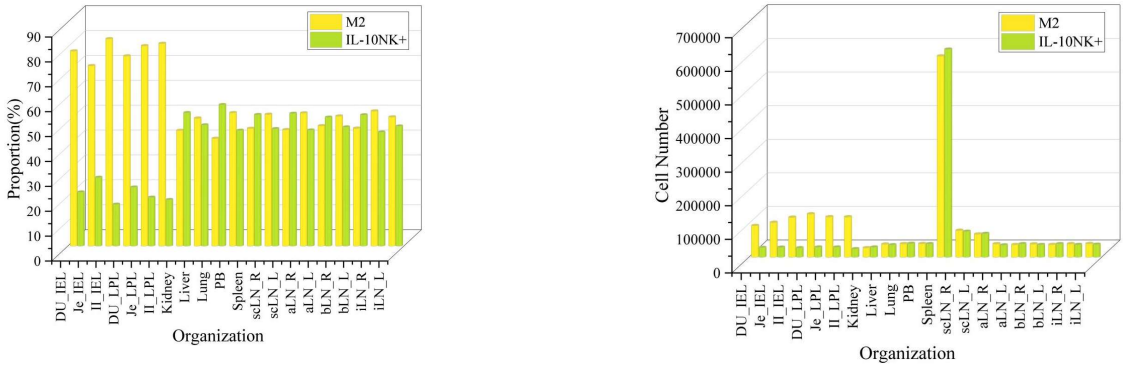

(a)Proportion (b)Quantity

Figure 6: Proportion and number of M2 macrophages and IL-10NK+ cells

IV. Conclusion

In this paper, a mathematical model of the tumor microenvironment was constructed, and a physical simulation method was combined to explore the distribution mechanism of immune cells in the NSCLC tumor microenvironment.

The average densities of TAMs in the three subpopulations of CD68+ TAMS, CD163⁺ TAMS, and IRF8⁺ TAMs in the samples in this paper were 362.5±288.1/mm², 97.8±118.9/mm², and 109.5±126.4/mm², respectively. The mean minimum proximity distances were 197.9±144.7 μm, 38.2±24.5 μm, and 50.9±23.7 μm, respectively. The effective percentages were 28.66±20.15%, 17.2±9.4%, and 8.1±6.5%, respectively. It can be seen that the mean density, mean minimum neighbor distance, and effective percentage of CD68⁺ TAMS in patients were significantly higher than those of CD163⁺ TAMS and IRF8⁺ TAMs.

Analysis of the flow cytometry results showed that the percentage of M2 macrophages, IL-10NK$^+$ cells differed significantly in each tissue. The epithelial and lamina propria of duodenum, jejunum, and ileum had more than 50% of M2 macrophages, while the proportions of M2 macrophages, IL-10NK$^+$ cells were similar in blood-related tissues and lymph node tissues. There were some differences in the number of M2 macrophages and IL-10NK$^+$ cells isolated and purified from different tissues, and the highest number of both M2 macrophages and IL-10NK$^+$ cells was found in spleen tissues.

Acknowledgements

1. The Excellent Teaching Team Fund of the Cyan-Blue Project at Yangzhou Polytechnic College;

2. Scientific and Technological Innovation Team Building Program of Suzhou Vocational Health College (No. SZWZYTD202205);

3. The Youth Fund of the Cyan-Blue Project at Jiangsu Province (Su Teacher Letter [2022] No. 51).

References

[1] Torre, L. A., Siegel, R. L., & Jemal, A. (2016). Lung cancer statistics. Lung cancer and personalized medicine: current knowledge and therapies, 1-19.

[2] Schabath, M. B., & Cote, M. L. (2019). Cancer progress and priorities: lung cancer. Cancer epidemiology, biomarkers & prevention, 28(10), 1563-1579.

[3] Di Giuseppe, M., Ciacchini, R., Micheloni, T., Bertolucci, I., Marchi, L., & Conversano, C. (2018). Defense mechanisms in cancer patients: a systematic review. Journal of psychosomatic research, 115, 76-86.

[4] Stankovic, B., Bjørhovde, H. A. K., Skarshaug, R., Aamodt, H., Frafjord, A., Müller, E., ... & Corthay, A. (2019). Immune cell composition in human non-small cell lung cancer. Frontiers in immunology, 9, 3101.

[5] Kargl, J., Busch, S. E., Yang, G. H., Kim, K. H., Hanke, M. L., Metz, H. E., ... & Houghton, A. M. (2017). Neutrophils dominate the immune cell composition in non-small cell lung cancer. Nature communications, 8(1), 14381.

[6] Mittal, V., El Rayes, T., Narula, N., McGraw, T. E., Altorki, N. K., & Barcellos-Hoff, M. H. (2016). The microenvironment of lung cancer and therapeutic implications. Lung cancer and personalized medicine: novel therapies and clinical management, 75-110.

[7] Wang, M., Zhu, L., Yang, X., Li, J., Liu, Y. E., & Tang, Y. (2023). Targeting immune cell types of tumor microenvironment to overcome resistance to PD-1/PD-L1 blockade in lung cancer. Frontiers in Pharmacology, 14, 1132158.

[8] Tan, Z., Xue, H., Sun, Y., Zhang, C., Song, Y., & Qi, Y. (2021). The role of tumor inflammatory microenvironment in lung cancer. Frontiers in pharmacology, 12, 688625.

[9] Dajon, M., Iribarren, K., & Cremer, I. (2015). Dual roles of TLR7 in the lung cancer microenvironment. Oncoimmunology, 4(3), e991615.

[10] Kwiecień, I., Polubiec-Kownacka, M., Dziedzic, D., Wołosz, D., Rzepecki, P., & Domagała-Kulawik, J. (2019). CD163 and CCR7 as markers for macrophage polarisation in lung cancer microenvironment. Central European Journal of Immunology, 44(4), 395-402.

[11] Tuminello, S., Veluswamy, R., Lieberman-Cribbin, W., Gnjatic, S., Petralia, F., Wang, P., ... & Taioli, E. (2019). Prognostic value of immune cells in the tumor microenvironment of early-stage lung cancer: a meta-analysis. Oncotarget, 10(67), 7142.

[12] Pullamsetti, S. S., Kojonazarov, B., Storn, S., Gall, H., Salazar, Y., Wolf, J., ... & Savai, R. (2017). Lung cancer–associated pulmonary hypertension: Role of microenvironmental inflammation based on tumor cell–immune cell cross-talk. Science Translational Medicine, 9(416), eaai9048.

[13] Wang, X., Chang, S., Wang, T., Wu, R., Huang, Z., Sun, J., ... & Mao, Y. (2022). IL7R is correlated with immune cell infiltration in the tumor microenvironment of lung adenocarcinoma. Frontiers in pharmacology, 13, 857289.

[14] Muppa, P., Terra, S. B. S. P., Sharma, A., Mansfield, A. S., Aubry, M. C., Bhinge, K., ... & Kosari, F. (2019). Immune cell infiltration may be a key determinant of long-term survival in small cell lung cancer. Journal of Thoracic Oncology, 14(7), 1286-1295.

[15] Liu, X., Wu, S., Yang, Y., Zhao, M., Zhu, G., & Hou, Z. (2017). The prognostic landscape of tumor-infiltrating immune cell and immunomodulators in lung cancer. Biomedicine & Pharmacotherapy, 95, 55-61.

[16] Zuo, S., Wei, M., Wang, S., Dong, J., & Wei, J. (2020). Pan-cancer analysis of immune cell infiltration identifies a prognostic immune-cell characteristic score (ICCS) in lung adenocarcinoma. Frontiers in immunology, 11, 1218.

[17] Engelhard, V. H., Rodriguez, A. B., Mauldin, I. S., Woods, A. N., Peske, J. D., & Slingluff Jr, C. L. (2018). Immune cell infiltration and tertiary lymphoid structures as determinants of antitumor immunity. The Journal of Immunology, 200(2), 432-442.

[18] Schneider, K., Marbaix, E., Bouzin, C., Hamoir, M., Mahy, P., Bol, V., & Grégoire, V. (2018). Immune cell infiltration in head and neck squamous cell carcinoma and patient outcome: a retrospective study. Acta oncologica, 57(9), 1165-1172.

[19] Xu, L., Yu, W., Xiao, H., & Lin, K. (2021). BIRC5 is a prognostic biomarker associated with tumor immune cell infiltration. Scientific reports, 11(1), 390.

[20] Lei, X., Lei, Y., Li, J. K., Du, W. X., Li, R. G., Yang, J., ... & Tan, H. B. (2020). Immune cells within the tumor microenvironment: Biological functions and roles in cancer immunotherapy. Cancer letters, 470, 126-133.

[21] Soo, R. A., Chen, Z., Teng, R. S. Y., Tan, H. L., Iacopetta, B., Tai, B. C., & Soong, R. (2018). Prognostic significance of immune cells in non-small cell lung cancer: meta-analysis. Oncotarget, 9(37), 24801.